Inorganic Chemistry

Article

pubs.acs.org/IC

Three Alkali-Metal–Gold–Gallium Systems. Ternary Tunnel Structures and Some Problems with Poorly Ordered Cations

Volodymyr Smetana, Gordon J. Miller,* and John D. Corbett*

Ames Laboratory-DOE and Department of Chemistry, Iowa State University, Ames, Iowa 50011, United States

Supporting Information

ABSTRACT: Six new intermetallic compounds have been characterized in the alkali metal (A = Na, Rb, Cs)–gold–gallium systems. Three isostructural compounds with the general composition $A_{0.55}Au_2Ga_2$, two others of AAu_3Ga_2 (A = Rb, Cs), and the related $Na_{13}Au_{41.2}Ga_{30.3}$ were synthesized via typical high-temperature reactions and their crystal structures determined by single-crystal X-ray diffraction analysis: $Na_{0.56(9)}Au_2Ga_2$ (**I**, *I*4/*mcm*, a = 8.718(1) Å, c = 4.857(1) Å, Z = 4), $Rb_{0.56(1)}Au_2Ga_2$ (**II**, *I*4/*mcm*, a = 8.950(1) Å, c = 4.829(1) Å, Z = 4), $Cs_{0.54(2)}Au_2Ga_2$ (**III**, *I*4/*mcm*, a = 9.077(1) Å, c = 4.815(1) Å, Z = 4), $RbAu_3Ga_2$ (**IV**, *Pnma*, a = 13.384(3) Å, b = 5.577(1) Å, c = 7.017(1) Å, Z = 4), $CsAu_3Ga_2$ (**V**, *Pnma*, a = 13.511(3) Å, b = 5.614(2) Å, c = 7.146(1) Å, Z = 4), $Na_{13}Au_{41.2(1)}Ga_{30.3(1)}$ (**VI**, *P6 mmm*, a = 19.550(3) Å, c = 8.990(2) Å, Z = 2). The first three compounds (**I**–**III**) are isostructural with tetragonal $K_{0.55}Au_2Ga_2$ and likewise contain planar eight-member Au/Ga rings that stack along c to generate tunnels and that contain varying degrees of disordered Na–Cs cations. The cation dispositions are much more clearly and reasonably defined by electron density mapping than through least-squares refinements with conventional anisotropic ellipsoids. Orthorhombic AAu_3Ga_2 (**IV**, **V**) are ordered ternary Rb and Cs derivatives of the $SrZn_5$ type structure, demonstrating structural variability within the AAu_3Ga_2 family. All attempts to prepare an isotypic "$NaAu_3Ga_2$" were not successful, but yielded only a similar composition $Na_{13}Au_{41.2}Ga_{30.3}$ ($NaAu_{3.17}Ga_{2.33}$) (**VI**) in a very different structure with two types of cation sites. Crystal orbital Hamilton population (COHP) analysis obtained from tight-binding electronic structure calculations for idealized **I**–**IV** via linear muffin-tin-orbital (LMTO) methods emphasized the major contributions of heteroatomic Au–Ga bonding to the structural stability of these compounds. The relative minima (pseudogaps) in the DOS curves for **IV** correspond well with the valence electron counts of known representatives of this structure type and, thereby, reveal some magic numbers to guide the search for new isotypic compounds. Theoretical calculation of total energies vs volumes obtained by VASP (Vienna Ab initio Simulation Package) calculations for KAu_3Ga_2 and $RbAu_3Ga_2$ suggest a possible transformation from $SrZn_5$- to $BaZn_5$-types at high pressure.

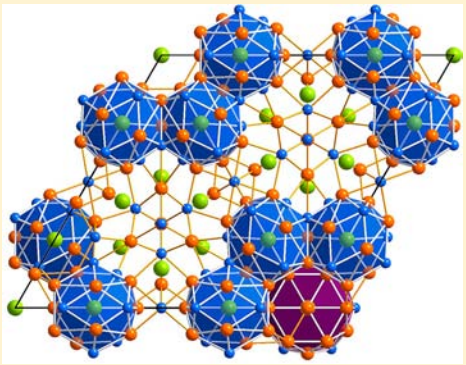

INTRODUCTION

Polar intermetallic compounds exhibit a large variety of novel structures with extensive variabilities of clusters and networks and interesting bonding features. These compounds form between metals or metalloids with widely different electronegativities, and many may be classified into one of two subgroups: polycationic networks with simple anions, or polyanionic networks with simple cations.[1] The latter include Zintl phases with closed-shell electronic configurations which often form with sufficiently large differences between the component atoms.[2,3] Electron-poorer polar intermetallic phases are electronically situated between Zintl and Hume–Rothery phases, and covalent bonding interactions between anionic and cationic parts may also be important. Examples of the latter are found among compounds between the alkali (*A*) or alkaline-earth (*Ae*) metals and later metals or metalloids and are often characterized by more delocalized bonding and substantial expansions of their coordination environments.[2−4] These also show metallic conductivity, in contrast to Zintl phases which belong to semiconductors. Addition of a third intermediate element to the former has proven to be a good way to expand the variety, and gold turns out to be a particularly good candidate[5] because of its novel bonding properties[6] and a capability to establish a diversity of bonding patterns. A large number of compounds within (A,Ae)–E–Tr systems (E = late transition element; Tr = triel) has been recently reported, mainly with In and Tl: K_3Au_5Tl,[7] Na_4AuTl,[8] Rb_2Au_3Tl,[8] $Na_{10}Ga_{10}Ni$,[9] $SrAu_4In_4$,[10] $Na_{13}(Cd,Tl)_{27}$,[11] $Ca_3Au_{12}Ga_7$,[12] BaPtIn.[13] Other investigations in A–Au–In systems have resulted in more novel structural and bonding features, e.g. $Na_2Au_6In_5$,[14] $NaAuIn_2$,[15] AAu_4In_6, $K_{1.76}Au_6In_4$, $K_xAu_2In_2$,[16] KAu_4In_2,[17] Na_3AuIn_2,[18] Na_3AuIn_2.[10] Almost all of them belong to the second type of polar intermetallics with polyanionic networks and clusters and simple cations, which are frequently encapsulated in the tunnels. $Na_{10}Ga_{10}Ni$ contains a polycationic network that surrounds $Ga_{10}Ni$ clusters.

Received: April 10, 2012
Published: June 27, 2012

   dx.doi.org/10.1021/ic300740u | *Inorg. Chem.* 2012, 51, 7711–7721

Table 1. Details of the Crystal Structure Investigations and Refinements for I −VI

empirical formula	$Na_{0.56(9)}Au_2Ga_2$ (**I**)	$Rb_{0.56(1)}Au_2Ga_2$ (**II**)	$Cs_{0.54(2)}Au_2Ga_2$ (**III**)	$RbAu_3Ga_2$ (**IV**)	$CsAu_3Ga_2$ (**V**)	$Na_{13}Au_{41.2(1)}Ga_{30.3(1)}$ (**VI**)
fw	546.13	581.24	605.48	815.81	863.25	10523.86
T (K)	293	293	293	293	293	293
wavelength (Å)	0.71073	0.71073	0.71073	0.71073	0.71073	0.71073
cryst syst	tetragonal	tetragonal	tetragonal	orthorhombic	orthorhombic	hexagonal
space group	*I*4/*mcm*	*I*4/*mcm*	*I*4/*mcm*	*Pnma*	*Pnma*	*P*6/*mmm*
a (Å)	8.718(1)	8.950(1)	9.077(1)	13.384(3)	13.511(3)	19.550(3)
b (Å)				5.577(1)	5.614(1)	19.550(3)
c (Å)	4.857(1)	4.829(1)	4.815(1)	7.017(1)	7.146(1)	8.990(2)
V (Å^3)	369.2(1)	386.8(1)	396.8(1)	523.7(2)	542.0(2)	2975.7(8)
Z	4	4	4	4	4	2
density (calcd) (g/cm^3)	9.83	9.98	10.14	10.35	10.58	11.74
μ (mm^{-1})	93.474	96.148	91.812	102.947	97.146	114.563
F(000)	904	963	999	1344	1416	8672
index ranges	$-11 \le h \le 11$	$-10 \le h \le 11$	$-10 \le h \le 11$	$-16 \le h \le 9$	$-17 \le h \le 11$	$-17 \le h \le 18$
	$-11 \le k \le 11$	$-11 \le k \le 11$	$-11 \le k \le 11$	$-6 \le k \le 6$	$-7 \le k \le 7$	$-15 \le k \le 18$
	$-6 \le l \le 6$	$-4 \le l \le 6$	$-6 \le l \le 3$	$-7 \le l \le 8$	$-9 \le l \le 9$	$-8 \le l \le 8$
no. of reflns collected	1486	1141	1127	2595	3007	4330
no. of indep. reflns	138	146	149	545	681	551
R_{int}	0.035	0.055	0.063	0.058	0.095	0.114
refinement method	full-matrix least-squares on F^2					
data/restr./params	138/0/13	146/0/13	149/0/13	545/0/34	681/0/35	551/0/83
GOF on F^2	1.09	1.16	1.28	1.15	1.13	1.36
final R indices ($I > 2\sigma(I)$)	$R1$ = 0.038, wR^2 = 0.079	$R1$ = 0.023, wR^2 = 0.051	$R1$ = 0.035, wR^2 = 0.083	$R1$ = 0.038, wR^2 = 0.073	$R1$ = 0.049, wR^2 = 0.093	$R1$ = 0.081, wR^2 = 0.127
R indices (all data)	$R1$ = 0.043, wR^2 = 0.083	$R1$ = 0.024, wR^2 = 0.052	$R1$ = 0.036, wR^2 = 0.083	$R1$ = 0.051, wR^2 = 0.078	$R1$ = 0.068, wR^2 = 0.111	$R1$ = 0.101, wR^2 = 0.133
largest diff. peak and hole (e$^-$/Å^3)	5.191 and −2.063	1.882 and −2.268	2.682 and −2.388	3.528 and −2.957	4.281 and −2.945	4.086 and −3.434

The A−Au−Ga systems were opened by earlier discoveries of four Li, Na, K and Rb compounds, Li_2AuGa,[19] $Na_{128}Au_{81}Ga_{275}$,[20] K_4Au_8Ga[21] and $RbAu_xGa_{3-x}$,[22] indicating a new direction for research, and these were followed by our complete investigation of the K−Au−Ga system and the discovery of four new network compounds: $K_{0.55}Au_2Ga_2$, KAu_3Ga_2, KAu_2Ga_4 and $KAu_{0.33}Ga_{2.67}$.[23] (Normally, Li shows completely different chemistry, and we do not include it in our work.) On the other hand, large variabilities among the binary compounds in the corresponding systems also have an influence on the diversity of the ternary neighbors. A number of compounds exist in the binary Au−Ga system together with a large solubility of Ga in Au around 350 °C, and this persists into ternary regions with alkali metals.[22,23] However, binary Au−Ga compounds are quite different from compounds that include more electropositive elements. Both heavy elements also form a few binary compounds with all of alkali metals,[24] which is a good sign for the formation of ternaries. The present extension of the K−Au−Ga explorations into Na, Rb and Cs systems has led to new and unexpected results and to more novel crystal structures: **I**, **II**, and **III** − nominally isostructural with $K_{0.55}Au_2Ga_2$[23] (and additional representatives of the $K_{0.5}Pt_2Si_2$[25] structure type) − but clear differences among the cation distribution details within the family have also been uncovered. Attempts to obtain isostructural examples of another K−Au−Ga representative of $BaZn_5$-type − KAu_3Ga_2,[23] resulted in $(Rb,Cs)Au_3Ga_2$ (**IV**, **V**), which are not isostructural but exhibit similar features and align with the neighboring $SrZn_5$ type.[26] Finally, a completely different sodium analogue,$Na_{13}Au_{41.2}Ga_{30.3}$ (**VI**), crystallizes in a larger structure that is, surprisingly, related to that of the electron-richer $Y_{13}Pd_{40}Sn_{31}$.[27]

EXPERIMENTAL SECTION

Synthesis. All materials were handled in a N_2-filled glovebox (≤0.1 ppm H_2O per volume). All compounds were obtained via standard high-temperature reactions of gold (99.995%, Ames Lab), gallium (99.99%, Alfa Aesar) and sodium, rubidium or cesium (99.9%, Alfa Aesar). Weighed amounts of the elements aimed at the stoichiometric compositions $A_{0.55}Au_2Ga_2$ and AAu_3Ga_2 that are known for potassium[23] were loaded with A = Na, Rb, or Cs and enclosed in tantalum tubes. These were welded and then sealed into evacuated fused silica ampules to protect them from air, as described previously.[28] The contents were prereacted at 500 °C for 12 h, cooled at 5−10 °C h^{-1} to 350 °C, equilibrated for 48−96 h, and slowly cooled to room temperature by switching off the furnace. The Na samples were heated at 500 °C for only 6 h to avoid reactions with Ta containers. The synthesis conditions chosen were similar to those used earlier for A−Au−In and K−Au−Ga systems.[18,23] Phase analyses of samples aimed at $A_{0.55}Au_2Ga_2$ (A = Na, Rb and Cs) (**I**−**III**) showed high yields (more than 90 mol. % on the basis of the powder X-ray pattern for $K_{0.55}Au_2Ga_2$[23]), whereas AAu_3Ga_2 (A = Rb and Cs, **IV**, **V**) were always obtained with 10 − 20 mol. % of the former type, perhaps because of incongruent melting. Single crystals were obtained for all products. In order to check for homogeneity regions in **I**−**III** samples, the compositions $A_{0.25}Au_2Ga_2$ and $A_{0.75}Au_2Ga_2$ were also reacted under the same conditions; however, only shifts in unit-cell parameters within acceptable 3σ limits were observed, similar to the behavior of $K_{0.55}Au_2Ga_2$. A negligible homogeneity region also exists for **VI** (~$Na_{13}Au_{41}Ga_{30}$, with two mixed Au/Ga positions) according to both X-ray single crystal and powder diffraction data. All compounds have metallic luster and are stable in moist air at room temperature for months.

dx.doi.org/10.1021/ic300740u | *Inorg. Chem.* 2012, 51, 7711−7721

Table 2. Atomic Coordinates and Equivalent Thermal Displacement Parameters for I − VI

atom	position	*x*	*y*	*z*	$U_{eq,iso}$* Å^2	SOF≠1[a]
			$Na_{0.56}Au_2Ga_2$ (**I**)			
Au	8*h*	0.31597(8)	0.18403(8)	1/2	0.0113(4)	
Ga	8*h*	0.3893(2)	0.1107(2)	0	0.0095(7)	
Na	8*f*	0	0	0.25 ± 0.13(2)	0.07(5)	0.28(5)
			$Rb_{0.56}Au_2Ga_2$ (**II**)			
Au	8*h*	0.31672(4)	0.18328(4)	1/2	0.0094(3)	
Ga	8*h*	0.3895(1)	0.1105(1)	0	0.0066(4)	
Rb	4*c*	0	0	0	0.32(3)	0.56(1)
			$Cs_{0.54}Au_2Ga_2$ (**III**)			
Au	8*h*	0.31714(8)	0.18286(8)	1/2	0.0114(5)	
Ga	8*h*	0.3892(2)	0.1108(2)	0	0.0097(7)	
Cs	4*c*	0	0	0	0.143(8)	0.54(2)
			$RbAu_3Ga_2$ (**IV**)			
Au1	4*c*	0.28395(8)	1/4	0.3911(1)	0.0076(3)	
Au2	4*c*	0.28849(8)	1/4	0.8017(1)	0.0090(3)	
Au3	4*c*	0.49332(8)	1/4	0.9245(1)	0.0086(3)	
Ga1	8*d*	0.1533(2)	0.9983(3)	0.6053(2)	0.0067(4)	
Rb1	4*c*	0.5720(2)	1/4	0.4017(3)	0.0139(6)	
			$CsAu_3Ga_2$ (**V**)			
Au1	4*c*	0.28045(9)	1/4	0.3778(1)	0.0120(3)	
Au2	4*c*	0.28695(9)	1/4	0.7950(1)	0.0151(3)	
Au3	4*c*	0.49418(9)	1/4	0.9307(1)	0.0110(3)	
Ga1	8*d*	0.1549(2)	0.9989(4)	0.5948(3)	0.0088(5)	
Cs1	4*c*	0.5693(2)	1/4	0.4075(2)	0.0143(4)	
			$Na_{13}Au_{41.2}Ga_{30.3}$ (**VI**)			
Au1	6*l*	0.1402(2)	0.8598(2)	0	0.019(2)	
Au2	2*d*	1/3	2/3	1/2	0.029(3)	
Au3	6*j*	0.4172(3)	0	0	0.020(2)	
Au4	12*q*	0.2334(3)	0.9146(3)	1/2	0.023(1)	
Au5	12*o*	0.2636(1)	0.7364(1)	0.1583(4)	0.019(1)	
Au6	12*o*	0.0899(2)	0.9101(1)	0.2673(5)	0.030(1)	
Au7	24*r*	0.3419(2)	0.8964(2)	0.7269(3)	0.022(1)	
Au8	6*m*	0.4532(2)	0.9064(4)	1/2	0.021(2)	
Au9/Ga9	6*j*	0	0.8667(6)	0	0.029(5)	0.35/0.65(5)
Au10/Ga10	1*a*	0	0	0	0.029(5)	0.28/0.72(5)
Ga1	6*k*	0.3839(8)	0	1/2	0.021(2)	
Ga2	12*o*	0.1781(3)	0.8219(3)	0.741(1)	0.012(3)	
Ga3	6*i*	1/2	0	0.237(2)	0.021(5)	
Ga4	2*c*	1/3	2/3	0	0.020(8)	
Ga5	12*p*	0.4137(7)	0.1329(7)	0	0.018(3)	
Ga6	6*k*	0.1621(9)	0	1/2	0.030(4)	
Ga7	12*o*	0.2159(7)	0.6080(4)	0.685(1)	0.016(3)	
Na1	6*m*	0.241(2)	0.759(2)	0.5	0.03(1)*	
Na2	2*e*	0	0	0.314(16)	0.08(5)*	
Na3	12*n*	0.268(2)	0	0.808(4)	0.03(1)*	
Na4	6*l*	0.579(3)	1.158(6)	0	0.08(3)*	

X-ray Diffraction Studies. Powder diffraction data were collected at 290 K with the aid of a Huber 670 Guinier powder camera equipped with an area detector and Cu K_α radiation (λ = 1.54059 Å). The samples were dispersed on Mylar sheets with the help of vacuum grease and fixed using split Al rings. The lattice parameters were refined using the WinXPow program.[29] Single crystals were fixed on glass fibers. Single-crystal diffraction data for **I** to **V** were collected at 293 K with Mo K_α radiation on a Bruker SMART APEX CCD diffractometer in the form of three sets of 606 frames with 0.3° scans in ω and exposures of 10 s per frame. The reflection intensities were integrated with the SAINT program in the SMART software package[30] over the entire reciprocal sphere. Empirical absorption corrections were accomplished with the aid of the SADABS program.[31] Single crystal diffraction data for the larger cell of **VI** were collected on a Stoe IPDS-II diffractometer. The data set came from a total of 360 frames with 0.5° scans in ω, and exposures of 8 min per frame. The starting atomic parameters derived via direct methods and the program SIR 97[32] were subsequently refined using the program SHELX-97[33] (full-matrix least-squares on F^2) with anisotropic atomic displacement parameters for all atoms in **I**−**VI** (except for Na in **VI**) in space groups *I*4/*mcm* (**I**−**III**), *Pnma* (**IV**, **V**), and *P*6/*mmm* (**VI**) within the WinGX program package.[34] Some details of data collection and refinement parameters are in Table 1. A somewhat large residual electron density of 5.19 e^-/Å^3 in **I** that is less than 1 Å from Au cannot be interpreted as any atom and probably results from an inadequate absorption correction for the heavy atom.

The atomic positions and equivalent displacement parameters are in Table 2. The anisotropic parameters of all independent atoms and additional crystallographic information are provided in Supporting Information. As a result of this investigation, $A_{0.55}Au_2Ga_2$ (A = Na, Rb,

dx.doi.org/10.1021/ic300740u | Inorg. Chem. 2012, 51, 7711−7721

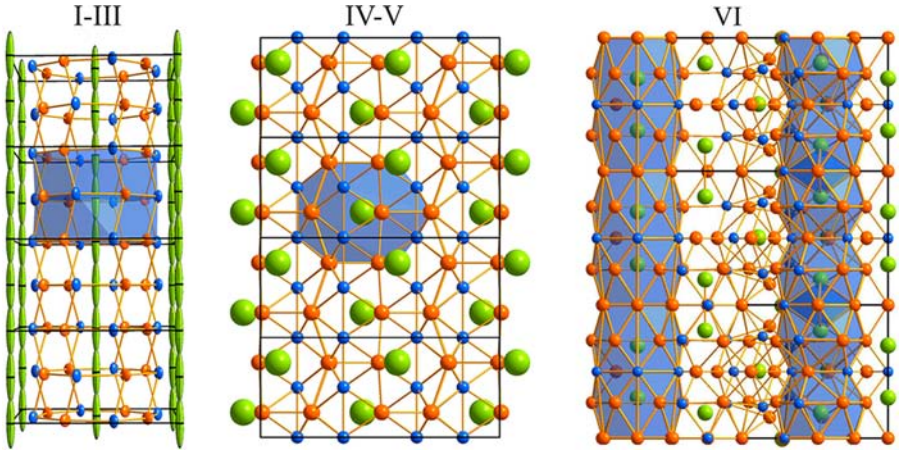

Figure 1. Crystal structure representations of $A_{0.55}Au_2Ga_2$ (**I**–**III**, [100], *I*4/*mcm*), AAu_3Ga_2 (**IV**–**V**, [001], *Pnma*) and $Na_{13}Au_{41.2}Ga_{30.3}$ (**VI**, [100], *P6*/*mmm*) with shaded polyhedra around alkali metal positions. The A (Na, Rb, or Cs), Au, and Ga atoms are light green, orange, and blue, respectively.

Cs) were found to be isostructural with $K_{0.55}Au_2Ga_2$; on the other hand, four phases around AAu_3Ga_2 (A = Na–Cs) crystallize in three different structure types, the highest symmetry being for KAu_3Ga_2 (*Cmcm*).[23]

Electron Microscopy. Atomic compositions of $Na_{0.53(5)}Au_2Ga_2$ and $Rb_{0.55(2)}Au_2Ga_2$ were secured from energy-dispersive X-ray analyses (EDX) on a JEOL 840A scanning electron microscope with an IXRF X-ray analyzer. Corrections were made for atomic number, absorption, and fluorescence. The compositions for both compounds obtained from the EDX analyses agree with the results obtained in the single crystal X-ray refinements; however, the accuracy of the latter Na measure was also not high.

Electronic Structure Calculations. Tight-binding calculations for **I**, **II**, **IV**, and **VI** were performed according to the linear muffin-tin-orbital (LMTO) method in the atomic sphere approximation (ASA).[35] (The first two were idealized by changing the diffuse fractional cations to those with unit occupancies at nearby higher symmetry points.) The radii of the Wigner-Seitz spheres were assigned automatically so that the overlapping potentials would be the best possible approximations to the full potentials.[36] They were determined as 1.51, 1.44, and 2.16 Å for Au, Ga, and Na, respectively, in **I**; 1.53 Å for Au, 1.47 Å for Ga, and 2.21 Å for Rb in **II**; 1.53 Å for Au, 1.47 Å for Ga, and 2.07 Å for Rb in **IV**; and 1.53–1.60, 1.47–1.52, and 2.01 Å for Au, Ga, and Na, respectively, in **VI**. Three empty spheres each for **I** and **II** and nine for **IV** were necessary in order to fill space within 16% or 18% overlap restrictions, respectively. Basis sets for Na 3s,3p, Rb 5s, 5p, (4d), Au 6s,6p,5d,(4f), Ga 4s,4p,(3d) (downfolded orbitals in parentheses) were employed. Scalar relativistic corrections were included to gain important aspects of gold's relativistic effects. For bonding analyses, the energy contributions of all filled electronic states for selected atom pairs were calculated as a function of energy by the COHP method (crystal orbital Hamilton population) and the energy-weighted sums, –ICOHP, from these.[37]

The Vienna ab initio simulation package (VASP)[38–40] was used to optimize the AAu_3Ga_2 (A = K–Rb) structures and to calculate the total energies of the known and hypothetical structures ($RbAu_3Ga_2$ model for KAu_3Ga_2, KAu_3Ga_2 model for $RbAu_3Ga_2$ and idealized $RbGa_4Au_4$). The projector augmented-wave (PAW)[41] pseudopotentials were adopted with the Perdew-Berke-Ernzerhof generalized gradient approximation (PBE-GGA),[42] in which scalar relativistic effects[43] are included. The conjugate algorithm[44] was applied for structural optimization with 4 × 5 × 8 and 4 × 8 × 5 Monkhorst-Pack mesh[45] to sample the first Brillouin zone for KAu_3Ga_2 and $RbAu_3Ga_2$, respectively, and a 4 × 4 × 6 mesh for all idealized AAu_4Ga_4 compounds. The atomic coordinates, volumes, and the aspect ratios of the unit cells for four different models were optimized before calculating the total energies. Total energies of the real and hypothetical structures of AAu_3Ga_2 were calculated over certain ranges of volumes to investigate their energy–volume dependences. The total energies of AAu_4Ga_4 were calculated for different cation positions along the *c* axis.

RESULTS AND DISCUSSION

Crystal Structures. Figure 1 shows composite views of the anionic network structures with their encapsulated cations as left: $A_{0.55}Au_2Ga_2$ (A = Na, Rb, Cs; **I**–**III**), middle: AAu_3Ga_2 (A = Rb, Cs; **IV**–**V**), and right: $Na_{13}Au_{41.2}Ga_{30.3}$ (**VI**). All are projections normal to the (vertical) tunnels and with neighboring polyhedra about the cations shaded in blue. All results for the crystal structure refinements of **I**–**VI** are summarized in Table 1, and the atomic coordinates, equivalent displacement parameters, and the A-site occupancies are listed in Table 2.

Tetragonal $\mathbf{A_{\sim 0.55}Au_2Ga_2}$ (**I**–**III**) (A = Na, Rb, Cs) phases were straightforwardly discovered by searching for the alkali-metal phases comparable to the recently discovered $K_{0.55}Au_2Ga_2$[23] (*I*4/*mcm*). A composite view of the refined results with Na is given in Figure 1 (left) together with the extreme anisotropic ellipsoids refined for Na. All three phases contain comparable, well-defined chains of Ga_4/Au_4 tetrahedral stars (TSs) connected along *c* via direct Au–Ga and Au–Au bonds to define tunnels; note, however, that the same assembly can also be generated through bonding between planar eight-membered rings of alternating Au/Ga atoms stacked along the *c* axis. Because we have shorter Au–Ga distances within the tetrahedral stars and shorter Au–Au between them, both ways are acceptable for the description. Broad electron density peaks that are separated by diffuse electron density distributions within these tunnels (below) result in marginal refinements of discrete cation positions therein and very elongated anisotropic displacement ellipsoids, increasingly so for the heavier alkali metals. The crystal data given in Table 2 for **I**, **II**, and **III** resulted from classical ellipsoidal refinements of either 8*f* (1/4 occupied) (0, 0, ± *z*; 0, 0, 1/2 ± *z*) sites for Na (and K[22]) or 4*c* (1/2 occupied) (0,0,0; 0,0,1/2) sites for Rb and Cs. These all result in characteristically extreme anisotropic ellipsoids for the cations with aspect ratios (U_{33}/U_{11}) that increase from ∼11 for Na to over 130 for Cs. The necessary differences in Wyckoff sites employed depends on whether the most probable cation sites lie around *c* = 0, 1/2, 1 (4*c*), coplanar with Au and Ga layers or, perhaps more normally, midway between these in

dx.doi.org/10.1021/ic300740u | *Inorg. Chem.* 2012, 51, 7711–7721

cavities at $z = \pm 1/4, 3/4$ (8*f*). However, the latter sites yield somewhat nonsensical distributions for Na, $z = \pm [0.25 \pm 0.13(2)]$.

The foregoing procedure is perhaps adequate for estimating cation proportions, but such descriptions in terms of anisotropic ellipsoids that may extend for several unit cells in $\pm z$ and interpenetrate substantially would appear to be undiscriminating ways to describe ranges of and variations in diffuse electron densities in these tunnels, and thereby, the nature of the disorders. On the other hand, electron density Fourier maps computed on the basis of observed reflection data, only the phases of *F* being assigned according to positional input for the heavy atoms, provide much more useful information about the nature of such disorders according to conventional X-ray scattering. Figure 2 shows (200) sections of

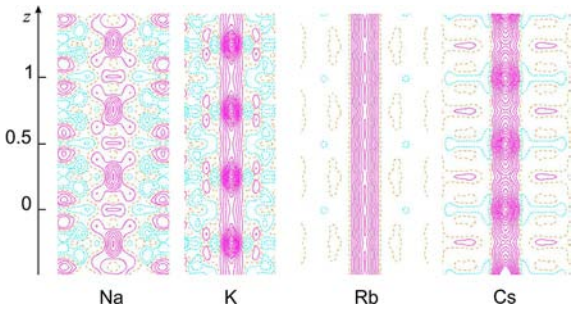

Figure 2. Electron density sections though the vertical *c* axes of the $A_{0.55}Au_2Ga_2$ phases (*I4mcm*): (left to right). A = Na, K,[22] Rb, Cs. The contour levels are 2.5, 1.6, 2.5, and 3.2 $e^-/Å^3$, respectively, with blue lines for negative values.

electron densities along the *c* axes for, left to right, $Na_{0.55}Au_2Ga_2$, $K_{0.55}Au_2Ga_2$, $Rb_{0.55}Au_2Ga_2$, and $Cs_{0.55}Au_2Ga_2$ (the e.d. map for the K phase was not reported previously[23]). The outlying Ga and Au atoms lie in layers at $z = 0, 1/2, 1$ but the atoms themselves are also alternately displaced above and below these sections, whereas the e.d. maxima for Na and K clearly lie at $z \approx 1/4, 3/4$ in the nominal cavities between the heavy atom layers. A similar behavior was observed for $K_{0.5}Pt_2Si_2$.[24] This is not true for Rb, for which the electron density appears to be nearly uniformly distributed in the cylindrical tunnel, perhaps slightly greater at $z \sim 0$, whereas Cs density is clearly greater around the planes of Au, Ga network atoms at $z \sim 0$. Remember that all of these represent averages of static, long-range, statistical disorders, for which the alternative difference (ΔF) map could be confusing. Note also that the contour levels in each part of Figure 3 were selected in order to define the range of cation distributions fairly uniformly, which means that background densities for atoms in the anionic networks tend to drop out as the cations become electron richer.

These characteristics suggest substantial ordering effects in which moderately rigid anionic networks define rather uniform tunnels in which the cations are somewhat loosely bound and poorly differentiated. The cations are still necessary for neutrality, and their filling of the preformed tunnel does contribute to overall stability. Changes in the lattice dimensions down the series are relatively small in the *c* direction, but more visible in *a*. The *a* and *c* axes vary by only +0.36 and −0.05 Å (4.4 and −1.0%) overall, which are accommodated in part by very small changes in the rhombus angles in the stars and (in part) by 0.08, −0.02, and 0.06 Å changes in the shortest A−Ga, Au−Au, and Au−Ga distances. (The irregular value for the Au−Au distance variation occurs entirely in the last step to Cs.) It should be noted that there is no cation location along the *c* axis at which the A−Au or A−Ga distances would betoo short. The distances from hypothetical 0 0 0 intralayer cation position to the surrounding Au and Ga are d_{A-Au} = 3.18−3.32 Å and above 4 Å for Ga. Although the composite of such effects in the lattice has a complex origin, the overall volume changes give a simpler focus. Each step of the overall 27.6 $Å^3$ (7.2%) volume increase down the series amounts to only 30 to 50% of the changes predicted according to Biltz[46] volume increments between alkali metal cations, values determined on the basis of a broad examination of conventional "salt" volumes. In other words, it appears that some free volumes are already present, intrinsic to the disordered states.

The observed electron density variations along the series, Figure 2, very much express a similar behavior; first, that the effective diameters and regularities of the tunnels together with the supposed electrostatic interactions of cations with the anions, Au particularly, provide little definition of local minima, especially for the larger alkali metals. The Na and K e.d. maps, which indicate that these are loosely bound in more or less conventional cavities in the $(Au_4Ga_4)_n$ tunnels with respect to the anion layers, at least seem plausible. The Rb and especially the Cs results require more interpretations or rationalizations since the maximum electron densities appear to be coplanar with the mixed Au/Ga layers defining the tunnels. The entire series gives the clear impression that decreasing cation binding energy down the series is the controlling factor.

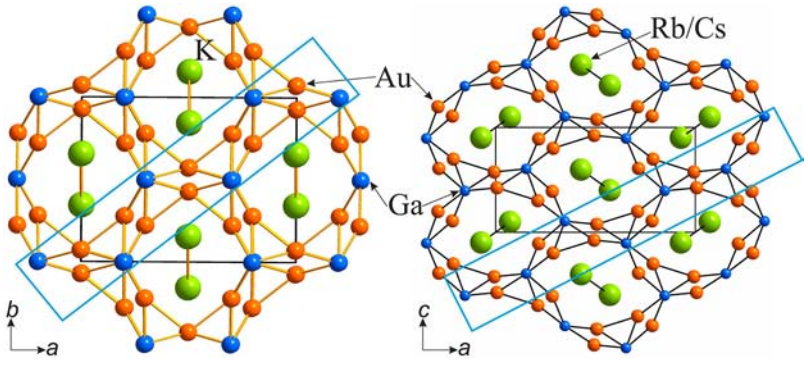

Figure 3. Crystal structures of KAu_3Ga_2[22] and $RbAu_3Ga_2$ (**IV**) viewed along tunnel axes with elements of the CrB and FeB crystal structures outlined in blue. The green atoms lie in nonbonded zigzag chains of cations.

dx.doi.org/10.1021/ic300740u | *Inorg. Chem.* 2012, 51, 7711−7721

Orthorhombic **$RbAu_3Ga_2$** (**IV**) and **$CsAu_3Ga_2$** (**V**) (Figure 1, middle) crystallize with the primitive orthorhombic structure of $SrZn_5$,[24] a derivative of *C*-centered orthorhombic $BaZn_5$[47] and are the first ternary representatives of the former. After the discovery of KAu_3Ga_2 in the latter structure type,[23] we imagined that isostructural compounds with other alkali metals could also exist, and the first single crystal from a reaction aimed at the stoichiometric composition $RbAu_3Ga_2$ gave similar unit cell parameters but for a primitive rather than a *C*-centered unit cell. Structures **IV** and **V** contain building units that are naturally very similar to those in KAu_3Ga_2[23] and $BaZn_5$;[47] however, the mutual orientations of these units is somewhat different. Although all of the zigzag A−A chains lie parallel to the *bc* planes in KAu_3Ga_2,[23] these are oriented at 108.3° to one another in **IV** and **V**, as contrasted in tunnel projections in Figure 3, left and right. Another interesting fact: the secondary K−K separations in the zigzag chains in the first KAu_3Ga_2, 3.83 Å, are definitely larger than Rb−Rb (3.66 Å) and Cs−Cs (3.62 Å) in **IV** and **V**, respectively, reflecting packing differences in the networks. The packing in **IV** and **V** remain relatively dense with no large voids in the structures. Coordination numbers of Au and Ga positions by all three elements are 11 and 12 as pentacapped trigonal prisms and strongly distorted icosahedra, respectively. The Au−Au and Au−Ga separations in **IV** and **V** lie in the ranges of 2.873(2)−3.018(1) and 2.578(2)−2.700(2) Å, comparable to 2.950(5)−3.007(4) and 2.592(6)−2.706(7) Å, respectively, in the higher symmetry KAu_3Ga_2. The splitting of the zinc sites in $SrZn_5$ on forming $RbAu_3Ga_2$ is such that the 8*d* sites that have eight Au and Sr neighbors are taken by gallium. The driving force would appear to be the greater number of polar Au−Ga bonds to each of the 8*d* Ga atoms, six, rather than three or four Ga neighbors about each of the three 4*c* Au atoms. All of these AAu_3Ga_2 structures could also be presented as derivatives of the simpler, hexagonal $CaCu_5$[48] (see Figure S2 in the Supporting Information). In the projection normal to the tunnel axes, Figure 3, both KAu_3Ga_2 and $RbAu_3Ga_2$ show splitting of $CaCu_5$ positions and deviations from the hexagonal angle, respectively, of 105.1 and 124.6°. Interestingly, binary AAu_5[49] compounds also crystallize in the $CaCu_5$-type; however, no such example has been found with Na. Selected representatives of the $CaCu_5$ type are summarized in the Table 3 and will be discussed later. It should also be noted that a structural relationship also exists between KAu_3Ga_2 and $RbAu_3Ga_2$ and the binary borides CrB[58] and FeB,[59] which crystallize in same space groups, *Cmcm* and *Pnma*, respectively. That is, very similar structural fragments of the borides are also found in the polyanionic networks of KAu_3Ga_2 and $RbAu_3Ga_2$, as marked with blue rectangles in Figure 3.

$Na_{13}Au_{41.2}Ga_{30.3}$ (**VI**) resulted from all attempts to obtain a sodium phase isotypic with KAu_3Ga_2. **VI** crystallizes with hexagonal symmetry, *P6/mmm* (Z = 2) in its own structure type. A projection of the orthorhombic structure is shown in Figure 1, right. The more notable features of this include two different chains of vertex-sharing Au_4Ga_4 TS[60] along at x = 1/3, (2/3); y = 2/3, (1/3) in the center of the view in Figure 1 (right). (See also the 001 projection of this structure in the abstract figure.) Each chain consists of mutually penetrating pairs of outer Au and inner Ga tetrahedra in which the shared vertices along the chain alternate between Ga and Au, Figure 4. These generate some distortions and also allow additional Au−Au bonding between the TS that surround Ga bridges. The Au−Ga distances within the chains range from 2.577 to 2.760 Å and the added Au−Au bonds, 2.80 Å and up.

Table 3. Crystallographic Data for Selected Representatives of the $CaCu_5$ Structure Type[a]

	a (Å)	c (Å)	V (Å^3)	c/a	VE/f.u.	ref
$CaCu_5$	5.092	4.086	91.75	0.802	7.0	48
$SrCu_5$	5.261	4.058	97.27	0.771	7.0	48
$SrAg_5$	5.644	4.631	127.76	0.820	7.0	49
$BaAg_5$	5.803	4.612	134.5	0.794	7.0	50
KAu_5	5.663	4.483	124.51	0.791	6.0	51
$RbAu_5$	5.762	4.442	127.72	0.770	6.0	51
$CaZn_5$	5.390	4.246	106.81	0.787	12.0	52
$SrZn_5$	5.541	4.282	113.86	0.772	12.0	52
$LaCu_3Al_2$	5.297	4.196	101.96	0.792	12.0	53
$CeCu_3Al_2$	5.249	4.180	99.72	0.796	12.0	53
$CeAl_3Pt_2$	5.368	4.406	109.95	0.820	12.0	54
$NdPt_3Al_2$	5.383	4.494	112.78	0.834	9.0	55
$PrNi_3Al_2$	5.079	4.041	90.28	0.795	9.0	56
$PrAl_3Ni_2$	5.293	4.064	98.6	0.767	12.0	56
$CaAl_{2.8}Ag_{2.2}$	5.521	4.430	116.94	0.802	12.6	57
$LaPt_3Ga_2$	5.400	4.498	113.59	0.832	11.0	55
KAu_3Ga_2	6.108	4.016	129.75	0.657	10.0	This work
$RbAu_3Ga_2$	6.269	3.960	134.77	0.631	10.0	This work

[a]VE = number of valence s, p electrons.

The face-centered orthorhombic $Au_{10}Ga_4$ unit situated in the center of the cell, Figure 5a, is best described as a primitive Au_8 cube with two additional Au and four Ga atoms centering all faces. Of course, these units are not truly separate, and pairs of Au atoms over each Ga-centered face extend them the length of the cell along *c*. The remaining space is filled by two very similar tunnels that each contain encapsulated Na atoms (shaded areas in Figure 1c) and are separated from each other by anionic networks. There are minor disorder problems with two mixed positions of Au and Ga, M9 (6*j*) and M10 (1*a*).

The basic building units in these tunnels are $Na_2(Au,Ga)_{26}$ and $Na_2(Au,Ga)_{32}$ units (at $x = y = 0$), Figure 5 b, c. (These are also highlighted in Figure 1 (right)). These can be described in terms of parallel 4−6−6−6−4− and 7−6−6−6−7− membered rings, and each is quite symmetric, exhibiting D_{2h} and D_{3h} point groups, respectively. The Na−Na pair distances within the units are ∼3.45 Å, much less than between pairs along *c*. This clear differentiation is in large contrast to A−A separations in the other A−Au−Ga(In) compounds. (The two tunnels are highlighted in the projection of this structure that accompanies the abstract.)

An appreciable family of other large and rather similar structures, all in space group *P6/mmm*, is also known with vec values that range over approximately 300 ± 10% e$^-$/cell . These and some of their features are listed in Table 4 for the following discussion. For example, a quite similar structure exists for $Y_{13}Pd_{40}Sn_{31}$,[27] but this is noticeably electron-richer, 326 e$^-$/cell, compared with 290 in $Na_{13}Au_{41.2}Ga_{30.3}$ (Z = 2), largely because of the complete substitution of Y for Na. The Pd and Sn positions are fully occupied, whereas two mixed Au/Ga positions out of 10 total in the present compound still leave a comparable amount of gold and, evidently, stronger bonding therewith. The Au−Au and Au−Ga distances in **VI**, 2.85−2.94 and 2.55−2.85 Å, are also comparable to those for Pd−Pd and Pd−Sn in the historic parent phase, 2.81−2.98 and 2.61−2.88 Å, respectively. One additional Au/Ga position (Figure 5b) is responsible for the separation of Na pairs along the *c* axis, whereas all of the Na positions correspond to those of Y in

dx.doi.org/10.1021/ic300740u | Inorg. Chem. 2012, 51, 7711−7721

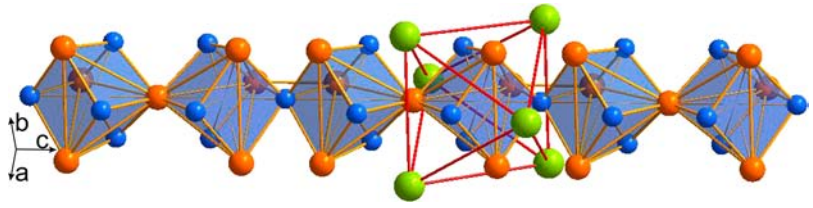

Figure 4. Chain of Au_4Ga_4 tetrahedral stars in the structure of **VI** that lie along the *c* axis. The highlighted intracluster Au−Au connections represent geometric tie-lines, not bonds, whereas the unmarked shorter intercluster Au−Au separations around bridging Ga (blue) are bonds.

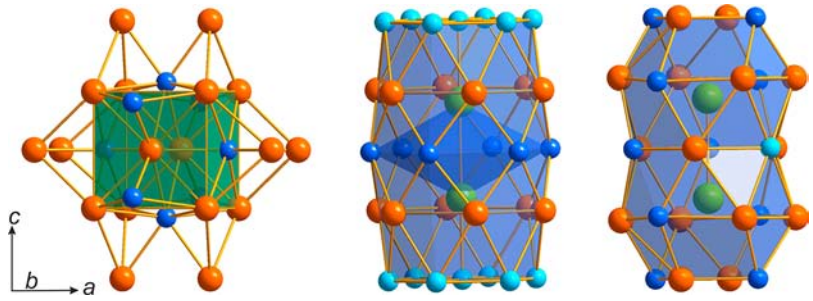

Figure 5. $Na_{13}Au_{41.2}Ga_{30.3}$ (**VI**) cell components. (Left) The central portion; (right) the two cluster units that encapsulate pairs of sodium ions. The latter appear on the left and right hand portion of Figure 1.

Table 4. Selected Features of the $Na_{13}Au_{41.2}Ga_{30.3}$ and Related Structure Types in Space Group *P6/mmm*, Arranged by Layering Sequence Sizes in the Polyhedra P1, P2 that Surround Cation Pairs

compd	*a* (Å)	*c* (Å)	*vec*	P1	P2	ref
$Na_{13}Au_{41.2}Ga_{30.3}$	19.550	8.990	290	4−6−6−6−4	7−6−6−6−7	this work
$Na_{26}Cd_{141}$	21.306	9.625	308	4−6−6−6−4	7−6−6−6−7	65
$Ca_{13}Ag_{46}In_{24.5}$	20.660	9.410	291	4−6−6−6−4	(6+)−6−6−6−(6+)	64
$Sc_{12.3}Ni_{40.7}Ge_{31}$	17.865	8.220	322	4−6−6−6−4	(6 + 1)−6−(6 + 1)	61
$Li_{13}Ni_{40}Si_{31}$	17.092	7.848	274	4−6−6−6−4	6−6−6−6−6	61
$Ta_{15.2}Co_{47.8}Si_{37}$	17.141	7.906	296	4−6−6−6−4	6−6−6−6−6	62
$Li_{13.5}Cu_{40.5}Si_{27}$	17.083	7.853	324	4−6−6−6−4	6−6−6−6−6	63
$Y_{13}Pd_{40}Sn_{31}$	19.891	9.246	326	4−6−6−6−4	6−6−6−6−6	27

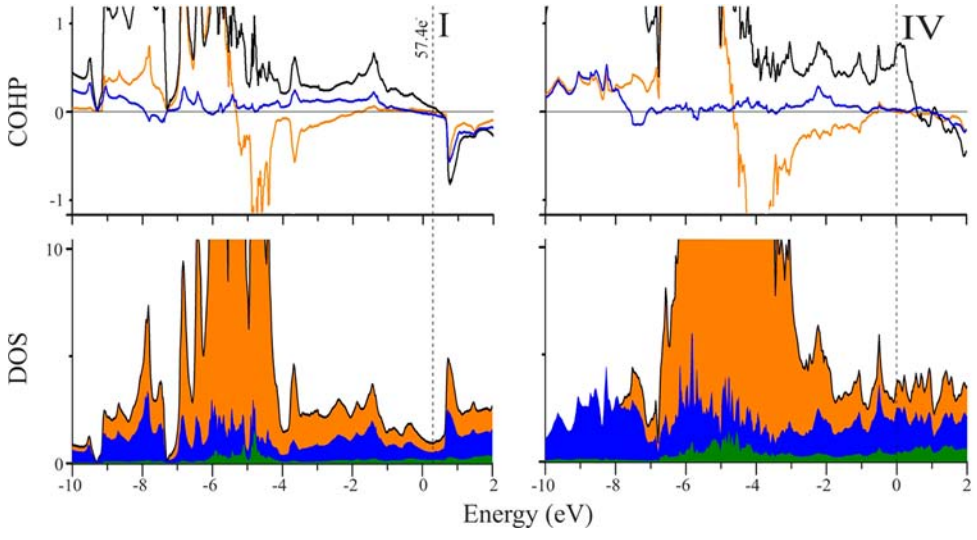

Figure 6. Results of LMTO-ASA calculations for idealized **I** ($NaAu_4Ga_4$) and **IV** ($RbAu_3Ga_2$) in the neighborhood of E_F. (Bottom) Total (black) and partial DOS curves for gold (orange), gallium (blue), and sodium (green). (Top) Total −COHP curves for three interactions for each structure (Au−Ga (black), Au−Au (orange), and Ga−Ga (blue)).

$Y_{13}Pd_{40}Sn_{31}$.The structural units are too large for useful calculations, but we imagine that the 13 Y atoms now on the former Na sites bind some or all of the additional 36 electrons, primarily in intermediate and largely nonbonding 4d and 5s states with other atoms. In three other compounds, $Li_{13}Ni_{40}Si_{31}$,$Ta_{15.2}Co_{47.8}Si_{37}$ and $Li_{13.5}Cu_{40.5}Si_{27}$,[61−63] which

dx.doi.org/10.1021/ic300740u | *Inorg. Chem.* 2012, 51, 7711−7721

evidently crystallize with $Y_{13}Pd_{40}Sn_{31}$ structure-type, we see only slight changes in cationic coordinates along the *c* axis at *x* = 0 and *y* = 0; however, they have a wide distribution of vec values, from 274 to 324. The only "black sheep" in the family might be a compound with general formula very similar to $Li_{13}Ni_{40}Si_{31}$: $Sc_{12.3}Ni_{40.7}Ge_{31}$. Crystallographically, this compound is very close to $Na_{13}Au_{41.2}Ga_{30.3}$ with only one significant difference − partial exchange of cations and anions, which implies local changes in site potentials as well. Formula similarities in this case do not show the main difference − that none of the cationic atom pairs observed for all other compounds along the *c* axis at *x* = 0 and *y* = 0 are present here. Instead, separate Sc atoms form polyhedra that can be described as face-centered hexagonal prisms $A(B)_{20}$, i.e., $Sc(Ni,Si)_{20}$ rather than $A_2(B)_{30}$ or $Y_2(Pd,Sn)_{30}$ units in $Y_{13}Pd_{40}Sn_{31}$ or $A_2(B)_{32}$ polyhedra found for $Na_2(Au,Ga)_{32}$ in $Na_{13}Au_{41.2}Ga_{30.3}$ (VI). These different polyhedra are designated under P2 in Table 4.

The recently published 291-electron $Ca_{13}Ag_{46}In_{24.5}$[64] is another relative with slightly different polyhedra and disordered Ca positions along the *c* axis instead of Na pairs (Figure 5). Another interesting and chemically simpler case with only a Cd anionic network is $Na_{26}Cd_{141}$, with 308 e^-/cell,[65] which is spatially closely related to **VI** (290 e^-). The tetrahedra in $Na_{26}Cd_{141}$ are also strongly distorted.

These few related compositions and structures suggest that an even wider range of isoelectronic compounds may be possible; however, examples of either other tetrels with alkali metals or triels with alkaline-earth elements and similar electron counts remain to be discovered. Theoretical comparisons among these and other relatives could be interesting and useful.

Electronic Structure and Chemical Bonding. The electronic densities-of-states (DOS) and near neighbor Au−Au, Au−Ga, and Ga−Ga COHP curves for idealized **I** ($Na_{0.5}Au_2Ga_2$) and **IV** ($RbAu_3Ga_2$) are shown in Figure 6, and their integrated −ICOHP results are summarized in Table 5. Both DOS curves exhibit broad valence *s,p* bands extending ca. 10 eV below the corresponding Fermi levels E_F, plus relatively narrow bands, over −6 to −4 eV for **I** and somewhat broader over −7 to −3 eV for **IV**. The latter bands originate from the Au 5*d* orbitals, which can be clearly identified via the Au−Au COHP curves. Both types exhibit low but nonzero DOS values around E_F that indicate metallic characteristics. According to the Au−Au, Au−Ga, and Ga−Ga COHP curves, both structural families have not quite achieved optimal orbital overlaps at these idealized chemical compositions by completely filling bonding states. Nevertheless, as typical for gold gallides and related phases, the largest −ICOHP values are found for Au−Ga and Au−Au near-neighbor contacts, which provide 89−93% of the total populations in the present examples. In all cases, an increase of the Fermi level from that of the idealized composition leads to decreases of DOS values, which can be achieved by adding valence electrons to AAu_4Ga_4 or removing them from $RbAu_3Ga_2$.

Table 5. Bond Length Ranges and Average −ICOHP Values in I, II, and IV

bond type	lengths (Å)	−ICOHP (eV/per avg bond)	*n*/cell	−ICOHP (eV/cell)	contribution (%)
		$Na_{0.5}Au_2Ga_2$(**I**)			
Au−Ga	2.531−2.648	1.31	48	62.88	80.9
Au−Au	2.923	0.995	8	7.96	10.2
Ga−Ga	2.730	0.63	8	5.04	6.5
Na−Au	3.251	0.1	12	1.2	1.5
Na−Ga	3.586	0.05	12	0.6	0.7
		$Rb_{0.5}Au_2Ga_2$(**II**)			
Au−Ga	2.587−2.718	1.43	48	68.74	83.1
Au−Au	2.936	1.02	8	8.16	9.9
Ga−Ga	2.801	0.62	8	4.92	5.9
Rb−Au	3.273	0.047	12	0.56	0.7
Rb−Ga	3.622	0.031	12	0.37	0.4
		$RbAu_3Ga_2$(**IV**)			
Au−Ga	2.589−2.746	1.168	48	56.08	75.4
Au−Au	2.904−3.041	0.658	20	13.17	17.7
Ga−Ga	2.795−2.819	0.525	8	4.21	5.7
Rb−Au	3.547−3.892	0.017	44	0.76	1.0
Rb−Ga	3.950−4.040	0.005	32	0.16	0.2

The DOS curves for **I**, as well as for **II**, decrease moderately beyond the Fermi levels for the idealized composition "$A_{0.5}Au_2Ga_2$", showing minima in these pseudogap regions at, respectively, ca. 0.36, 0.15, and 0.15 eV above E_F. These positions correspond to 28.7, 28.6, and 28.6 e^-/formula unit, respectively, which are slightly higher than both the idealized electron counts for "$A_{0.5}Au_2Ga_2$" of 28.5 e^- as well as those obtained by experiment, i.e., 28.56 e^- for A = Na or Rb and 28.54 e^- for A = Cs. Adding valence electrons to the ideal "$A_{0.5}Au_2Ga_2$" also increases the heteroatomic Au−Ga Hamilton populations, which are optimized at valence electron counts of about 28.58 e^-, 28.58 e^-,and 28.56 e^- for Na, K,[23] and Rb, respectively. These changes can be achieved by increasing the alkali metal contents, i.e., $A_{0.5+x}Au_2Ga_2$, as was marginally observed experimentally (Table 2), or by substitution of some Ga for Au, e.g, "$AAu_{2-y}Ga_{2+y}$. To check the second possibility, total energies for the optimized hypothetical models were calculated using VASP.[38−40] Switching only one of eight Au atoms per unit cell to Ga increases the total energies for the Na and K cases by ca. 0.45 eV/f.u.. Very similar destabilizations are achieved after completely interchanging Au and Ga positions and allowing optimization of the coordinates and cell volume. Optimization after interchanging Au and Ga positions leads to larger unit cell volumes because of longer Au−Au, as compared with Ga−Ga distances within the tetrahedral stars and smaller A−Ga than A−Au distances, which have never been observed for any ternary compound of these elements. With this result, total energy calculations were also performed on the observed network of Au and Ga atoms for different Na or Rb positions along the c axis between *z* = 0 and 0.5 in steps of 0.05 (see Figure S3 in the Supporting Information). The global minimum for the most probable cation position in both phases is at *z* = 0.25, which lies midway between the network layers and is 0.04 or 0.06 eV/f.u. more stable than that with the cations in the Au−Ga layers (*z* = 0) for Na and Rb, respectively. The former is as observed, Figure 2, whereas the e.d. results for the Rb phase do not really differentiate between *z* coordinates for the cation.

−ICOHP analyses of the $A_{\sim 0.55}Au_2Ga_2$ series (Table 4) reveal that larger Au−Ga and Au−Au populations occur for the short inter-TS bonds that lie in the tunnel walls around the Na, K cations, rather than for the longer Au−Ga and Au−Au contacts within the tetrahedral stars. Interestingly, a computational optimization using VASP of the hypothetical, isoelectronic structure "$Rb_{0.5}Cd_4$", in which all Cd atoms could be symmetry-equivalent (space group *I*4/*mmm*, rather than *I*4/*mcm* in Rb0.56Au2Ga2), resulted in the formation of

dx.doi.org/10.1021/ic300740u | *Inorg. Chem.* 2012, 51, 7711−7721

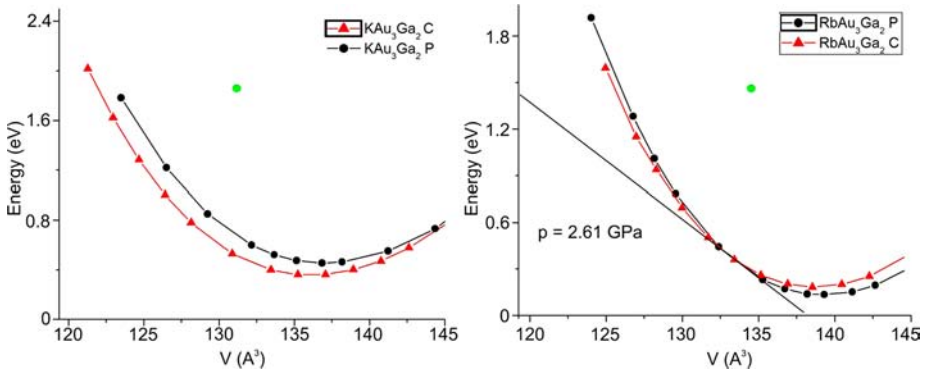

Figure 7. $E(V)$ curves of KAu_3Ga_2 and $RbAu_3Ga_2$ in both the primitive (black) and the *C*-centered (red) orthorhombic modifications ($SrZn_5$ and $BaZn_5$ types, respectively) as calculated with VASP. The green dot indicates the $E(V)$ minimum point for the corresponding compound in the hexagonal $CaCu_5$-type structure.

tetrahedral stars with segregation of Cd positions into two types with longer distances within and shorter distances between adjacent TSs, as observed. The sum of Au−Ga and Ga−Ga populations constitutes more than 90% of total −ICOHP values. Although homoatomic Au−Au and Ga−Ga interactions in **I** and **II** are substantially optimized at E_F, heteroatomic Au−Ga contacts remain bonding somewhat beyond E_F, especially for the Na compound (Table 6). The analysis of −ICOHP data for the individual bonds in **I** and **II** shows that those for Au−Ga and Au−Au, ∼1.3−1.4 and 1.0 eV/(bond mol), are nearly twice as large as those from Ga−Ga, 0.6 eV, and, additionally, the first occur six times more frequently than the second. Orbital interactions with Au atoms are always dominant contributions, evidently from enhanced (relativistic) 5d orbital participation in bonding. The −ICOHP values for all A−Ga and A−Au interactions are very small for all structures, no larger than 0.1 eV/bond·mol, indicating relatively weak cation−anion interactions in this family of compounds that also decrease with increasing cation sizes.

A slightly different situation is observed for orthorhombic $RbAu_3Ga_2$ (**IV**) because of its higher Au and lower Ga proportions and bond numbers. This result compares well with that for the related KAu_3Ga_2 phase,[23] which contains the same number of but differently oriented building units. The present Rb and Cs phases crystallize with somewhat lower symmetry, which leads to more Au−Ga and Ga−Ga differentiations with distance. The Au−Ga distances in **IV** range from 2.569 to 2.716 Å, and there are two different Ga−Ga separations, 2.770 and 2.807 Å, whereas there are only three Au−Ga and one Ga−Ga separations in KAu_3Ga_2. Both Au−Au and Ga−Ga bonding in **IV** are optimized at E_F, whereas Au−Ga interactions remain bonding up to ca. +1 eV (Figure 6), similar to the behavior of KAu_3Ga_2. The DOS values decrease significantly below the Fermi level, as with the two previous structures, with relative minima at the Fermi level and pseudogaps at ∼1 eV. The last corresponds to 12 valence s,p electrons per formula unit, in contrast to only 10 e^- in $RbAu_3Ga_2$. This suggests that substitutional tuning to this point might be useful. One example of this count is already known for the parent, $SrZn_5$,[26] probably indicating some magic count for this type of structure. As mentioned above, another decrease of the DOS can be achieved by removing some valence electrons, for example, by replacing Ga by Au as occurs in K−Au−Ga system.[23] The isotropic displacement parameter of Ga is slightly smaller than those of Au, perhaps indicating a mixed Au/Ga position; however, no Au could be refined at the Ga site.

Since $RbAu_3Ga_2$ (**IV**), $CsAu_3Ga_2$ (**V**), and KAu_3Ga_2[23] crystallize with very similar structures and unit cell volumes, we scanned their total energies vs volume using VASP. Before any total energy calculation was conducted, the unit cell volume, shape (i.e., c/a and b/a ratios), and atomic free coordinates were optimized for the *C*-centered KAu_3Ga_2-type and primitive $RbAu_3Ga_2$-type models for both elements. After that, all volume changes were allowed for fixed unit-cell shape and coordinates. These $E(V)$ curves are shown in Figure 7. Global minima are observed for the *C*-centered model in KAu_3Ga_2 and the primitive cell model in $RbAu_3Ga_2$, both in good agreement with the experimental results. The equilibrium volumes were always calculated to be slightly larger than the experimental volumes, viz., 543.9 vs 523.5 $Å^3$/cell for KAu_3Ga_2, and 557.5 vs 523.7 $Å^3$/cell for $RbAu_3Ga_2$, which might be caused by the PBE pseudopotentials used in the calculations. For KAu_3Ga_2, the *C*-cell offers lower total energies for all volumes scanned (Figure 7, left); however, a different situation is observed for $RbAu_3Ga_2$. The $E(V)$ curve suggests that a pressure-induced phase transition from the primitive to a *C*-centered structure may occur around 2.6 GPa. Of course, high pressure experiments are needed to confirm this computational prediction.

Because there is a close structural relationship between both orthorhombic AAu_3Ga_2 structure types and the hexagonal $CaCu_5$ structure type, total energies of hypothetical models of **IV** and **V** in the latter hexagonal modification were also evaluated. The Ca position was replaced by either K or Rb and the two Cu sites by corresponding Au and Ga atoms. Since all coordinates in the $CaCu_5$ type are fixed, only the unit cell volume and c/a ratios were optimized. Table 5 lists various examples adopting the $CaCu_5$-type structure, and shows that the observed c/a ratios vary within 3% around 0.80 for examples with widely different unit cell parameters and volumes. Reported $CaCu_5$-type structures also exist for 6−12 valence s,p electrons per formula unit, with most examples occurring for 6−7 e^- and 12 e^-. Structural optimization of 10 e^- KAu_3Ga_2 and $RbAu_3Ga_2$ converged on c/a ratios that are 20% smaller, i.e., ca. 0.65, but give cell volumes that are comparable to $SrAg_5$ and $BaAg_5$. These hexagonal models of KAu_3Ga_2 and $RbAu_3Ga_2$ gave total energies that exceeded the total energies of their corresponding orthorhombic forms by 0.34 and 0.42 eV/f.u., respectively. In addition, the optimized volumes are ca. 4% smaller than the experimental volume. The optimized total energies and volumes for these two points are included in Figure 7.

dx.doi.org/10.1021/ic300740u | *Inorg. Chem.* 2012, 51, 7711−7721

Finally, because of the large unit cell and complexity of the hexagonal $Na_{13}Au_{41.2}Ga_{30.3}$ (**VI**) structure, preliminary electronic structure calculations were performed with Au 5d orbitals taken as (pseudo) core orbitals to explore whether the DOS arising from just the valence s and p bands might indicate significant electronic origins to its structural stability. This choice was necessary because inclusion of Au 5d orbitals was prohibitively large to complete self-consistent calculations. Both mixed positions were assigned as either pure Ga or Au. The total DOS curve (see Figure S4 in the Supporting Information) is a continuous curve crossing the Fermi level, as for all previous compounds and the signature of metallic character. The total DOS is dominated by Au and Ga states, with valence *s* states mainly in the low energy region and valence p states around the Fermi level. The profile of the total DOS curve resembles a nearly free-electron system with some relative minima at the Fermi level, but no clear pseudogaps near the Fermi level for $Na_{13}Au_{41.2}Ga_{30.3}$ (**VI**). Valence electron counts for $Na_{13}Au_{41.2}Ga_{30.3}$ (290 e^-), $Na_{26}Cd_{141}$ (308 e^-), and $Y_{13}Pd_{40}Sn_{31}$ (326 e^-) are marked in Figure S4 with dotted lines, the last being close to a notable pseudogap. Thus, further theoretical examination of the electronic structure is necessary to identify the interatomic interactions and chemical bonding features that enhance the formation of this broad compound class presented in Table 4.

SUMMARY

Two series of compounds with compositions of about $A_{0.5}Au_2Ga_2$ (**I**–**III**) and AAu_3Ga_2 (**IV**, **V**) have been investigated for A = Na, Rb, and Cs. Although all $A_{0.5}Au_2Ga_2$ phases of the first type crystallize in the previously discovered tetragonal $K_{0.55}Au_2Ga_2$ type, the Au-richer AAu_3Ga_2 compositions were found to occur in three different structure types. $Na_{13}Au_{41.2}Ga_{30.3}$ has its own structure, similar to that of the electron-richer $Y_{13}Pd_{40}Sn_{31}$ and completely different from AAu_3Ga_2 (A = K, Rb, Cs). The last two are evidently the first ternary intermetallic representatives of the $SrZn_5$ structure type. Analysis of electronic structure calculations shows that all of the new compounds are metallic in nature, and that the principal Hamilton bond populations come from the polar Au–Ga bonds in the networks, with Au–Au bonding of secondary significance. An insidious feature of the refined crystal structures of **I**–**III**, $A_{0.55}Au_2Ga_2$, are the increasing diffuseness of the Na, K, Rb distributions, and a consequent decrease in the meaningfulness of refinements that utilize conventional anisotropic displacement parameters. Only a few other examples of these differences with disorder have been examined.[14,66]

ASSOCIATED CONTENT

Supporting Information

Table of distances in $RbAu_3Ga_2$ and $SrZn_5$; results of LMTO-ASA calculations for $SrZn_5$; result of the VASP optimization for different Na positions in the structure of $Rb_{0.5}Au_2Ga_2$; results of LMTO-ASA calculations for $Na_{13}Au_{41.2}Ga_{30.3}$; cif files. This material is available free of charge via the Internet at http://pubs.acs.org.

AUTHOR INFORMATION

Corresponding Author

*E-mail: jcorbett@iastate.edu (J.D.C); gmiller@iastate.edu (G.J.M.).

Notes

The authors declare no competing financial interest.

ACKNOWLEDGMENTS

The research was supported by the Office of the Basic Energy Sciences, Materials Sciences Division, U.S. Department of Energy (DOE). Ames Laboratory is operated for DOE by Iowa State University under contract No. DE-AC02-07CH11358.

REFERENCES

(1) Corbett, J. D. *Inorg. Chem.* **2010**, *49*, 13.
(2) Corbett, J. D. In *Chemistry, Structure and Bonding of Zintl Phases and Ions*; Kauzlarich, S., Ed.; VCH Publishers: New York, 1996, Chapter 3.
(3) Schafer, H.; Eisenmann, B.; Müller, W. *Angew. Chem., Int. Ed.* **1973**, *12*, 694.
(4) Corbett, J. D. *Angew. Chem., Int. Ed.* **2000**, *39*, 670.
(5) Lin, Q.; Corbett, J. D. *J. Am. Chem. Soc.* **2007**, *129*, 6789.
(6) Pyykkö, P. *Chem. Rev.* **1988**, *88*, 63.
(7) Zachwieja, U. *Z. Anorg. Allg. Chem.* **1997**, *623*, 1621.
(8) Li, B.; Kim, S.-J.; Miller, G. J.; Corbett, J. D. *Inorg. Chem.* **2009**, *48*, 6573.
(9) Henning, R. W.; Corbett, J. D. *Inorg. Chem.* **1999**, *38*, 3883.
(10) Li, B.; Corbett, J. D. *J. Am. Chem. Soc.* **2006**, *128*, 12392.
(11) Li, B.; Corbett, J. D. *Inorg. Chem.* **2004**, *43*, 3582.
(12) Lin, Q.; Corbett, J. D. *Inorg. Chem.* **2008**, *47*, 3462.(13).
(13) Palasyuk, A.; Corbett, J. D. *Z. Anorg. Allg. Chem.* **2007**, *633*, 2563.
(14) Li, B.; Corbett, J, D. *Inorg. Chem.* **2007**, *46*, 6022.
(15) Li, B.; Corbett, J. D. *J. Am. Chem. Soc.* **2006**, *128*, 12392.
(16) Li, B.; Corbett, J. D. *Inorg. Chem.* **2005**, *44*, 6515.
(17) Zachwieja, U. *J. Alloys Comp.* **1996**, *235*, 7.
(18) Zachwieja, U. *Z. Anorg. Allg. Chem.* **1995**, *621*, 1677.
(19) Pauly, H.; Weiss, A.; Witte, H. *Z. Metallkd.* **1968**, *59*, 47.
(20) Tillard-Charbonnel, M.; Belin, C. *Z. Kristallogr.*. **1993**, *206*, 310.
(21) Mueller, J.; Zachwieja, U. *Z. Anorg. Allg. Chem.* **2000**, *626*, 1867.
(22) Henning, R. W.; Corbett, J. D. *J. Alloys Compd.* **2002**, *338*, 4.
(23) Smetana, V.; Corbett, J. D.; Miller, G. J. *Inorg. Chem.* **2012**, *51*, 1695.
(24) *Binary Alloy Phase Diagrams*; Massalski, Th.B., Okamoto, H., Eds., 2nd ed.; ASM International: Metals Park, OH, 1994.
(25) Thronberens, W.; Sinnen, H. D.; Schuster, H. U. *J. Less-Common Met.* **1980**, *76*, 99.
(26) Wendorff, M.; Röhr, C. *Z. Naturforsch. B* **2007**, *62*, 1549.
(27) Cenzual, K.; Parthe, E. *Acta Crystallogr., Sect. C* **1984**, *40*, 1127.
(28) Dong, Z.-C.; Corbett, J. D. *J. Am. Chem. Soc.* **1993**, *115*, 11299.
(29) *WinXPow 2.10*; Stoe & Cie GmbH: Darmstadt, Germany, 2004.
(30) *SMART*; Bruker AXS, Inc.; Madison, WI, 1996.
(31) Blessing, R. H. *Acta Crystallogr.* **1995**, *A51*, 33.
(32) Altomare, A.; Burla, M.; Camalli, M.; Carroccini, B.; Cascarano, G.; Giacovazzo, C.; Guagliardi, A.; Moliterni, A.; Polidori, G.; Rizzi, R. *J. Appl. Crystallogr.* **1999**, *32*, 115.
(33) Sheldrick, G. M. *SHELXL-97: Program for the Refinement of Crystal Structures*; University of Göttingen: Göttingen, Germany, 1997.
(34) Farrugia, L. *J. Appl. Crystallogr.* **1999**, *32*, 837.
(35) Krier, G.; Jepsen, O.; Burkhardt, A.; Andersen, O. K. *TB-LMTO-ASA Program*, version 4.7; Max-Planck-Institut für Festkörperforschung: Stuttgart, Germany, 1995.
(36) Jepsen, O.; Andersen, O. K. *Z. Phys. B* **1995**, *97*, 35.
(37) Dronskowski, R.; Blöchl, P. E. *J. Phys. Chem.* **1993**, *97*, 8617.
(38) Kresse, G.; Hafner, J. *Phys. Rev. B* **1993**, *47*, 558.
(39) Kresse, G.; Furthmüller. *J. Comput. Mater. Sci.* **1996**, *6*, 15.
(40) Kresse, G.; Furthmüller. *J. Phys. Rev. B* **1996**, *54*, 11169.
(41) Kresse, G.; Joubert, D. *Phys. Rev.* **1999**, *59*, 1758.
(42) Perdew, J. P.; Burke, K.; Ernzerhof, M. *Phys. Rev. Lett.* **1996**, *77*, 3865.
(43) Pyykkö, P. *Chem. Rev.* **1988**, *88*, 563.

(44) Press, W. H.; Flannery, B. P.; Teukolsky, S. A.; Vetterling, V. T. in: *Numerical Recipes*, Cambridge University Press, New York, 1986.
(45) Monkhorst, H. J.; Pack, J. D. *Phys. Rev. B* **1976**, *13*, 5178.
(46) Biltz, W. *Raumchemie der festen Stoffe*; Leopold Voss Verlag: Leipzig, Germany, 1934, p 238.
(47) Baenziger, N. C.; Conant, J. W. *Acta Crystallogr.* **1956**, *9*, 361.
(48) Bruzzone, G. *J. Less-Common Met.* **1971**, *25*, 361.
(49) Heumann, T.; Harmsen, N. *Z. Metallkd.* **1970**, *61*, 906.
(50) Bruzzone, G.; Ferretti, M.; Merlo, F. *J.Less-Common Met.* **1987**, *128*, 259.
(51) Zachwieja, U. *J. Alloys Compd.* **1993**, *196*, 187.
(52) Wendorff, M.; Roehr, C. *Z. Naturforsch. B* **2007**, *62*, 1549.
(53) Bauer, E.; Gratz, E.; Keller, L.; Fischer, P.; Furrer, A. *Phys. B: Condens. Matter* **1993**, *186*, 608.
(54) Blazina, Z.; Westwood, S. M. *J. Alloys Compd.* **1993**, *201*, 151.
(55) Blazina, Z. *J. Alloys Compd.* **1994**, *216*, 251.
(56) Rykhal', R. M.; Zarechnyuk, O. S.; Kuten', Ya.I. *Dopov. Akad. Nauk Ukr. RSR A* **1978**, *40*, 1136.
(57) Cordier, G.; Doersam, G.; Friedrich, T.; Henseleit, R.; Roehr, C. *J. Alloys Compd.* **1993**, *190*, 201.
(58) Kiessling, R. *Acta Chem. Scand.* **1949**, *3*, 595.
(59) Bjurstroem, T.; Arnfelt, H. *Z. Phys. Chem.* **1929**, *4*, 469.
(60) Schubert, K., *Kristallstrukturen zweikomponentiger Phasen*; Springer: Berlin, 1964; p 150.
(61) Bodak, O; Pavlyuk, V; Andrusyak, R; Kotur, B; Pecharsky, V; Bruskov, V *Kristallografiya* **1990**, *35*, 312.
(62) Vilasi, M; Venturini, G; Steinmetz, B; Malaman, B *J. Alloys Compd.* **1995**, *227*, 32.
(63) Pavlyuk, V.; Kevorkov, D.; Bodak, O.; Pecharskii, V. *Kristallografiya* **1995**, *40*, 178.
(64) Lin, Q.; Corbett, J. D. *Inorg. Chem.* **2011**, *50*, 11091.
(65) Todorov, E; Sevov, S. C. *Inorg. Chem.* **1998**, *37*, 6341.
(66) Samal, S.; Lin Q.; Corbett, J. D. *Inorg. Chem.* **2012**, submitted for publication.